A&A 399, 763–772 (2003)
DOI: 10.1051/0004-6361:20021720

Astronomy & Astrophysics

Behaviour of Comet 21P/Giacobini-Zinner during the 1998 perihelion

L.-M. Lara[1], J. Licandro[2], A. Oscoz[3], and V. Motta[3,4]

[1] Instituto de Astrofísica de Andalucía, CSIC, Camino Bajo de Huétor 24, 18008 Granada, Spain
e-mail: lara@iaa.es
[2] Centro Galileo Galilei & Telescopio Nazionale Galileo PO Box 565, 38700 Santa Cruz de La Palma, Tenerife, Spain
e-mail: licandro@tng.iac.es
[3] Instituto de Astrofísica de Canarias, 38205 La Laguna, Tenerife, Spain
e-mail: aoscoz@ll.iac.es
[4] Departamento de Astronomía, Facultad de Ciencias, Universidad de la República, Iguá 4225, 11400 Montevideo, Uruguay
e-mail: vmotta@ll.iac.es

Received 4 March 2002 / Accepted 7 November 2002

Abstract. Comet 21P/Giacobini–Zinner was observed from Nov. 8 to Dec. 10, 1998. Pre- and post-perihelion CCD images of the gas (CN, C_2) and dust (green and red continua) coma were obtained with the 82 cm IAC-80 telescope at Teide Observatory (Canary Islands, Spain). For $v_p = 0.85 r_H^{-0.5}$ and $v_d = 1.19$ km s^{-1} (i.e. characteristic of HCN being the CN parent species), the CN column density profiles are best reproduced with parent and daughter lifetimes of the order of 19 300 and 256 000 s. An equally good reproduction of the observed profiles is achieved by considering that a mixture of nitrogen compounds expanding at $v_p = 1$ km s^{-1} and with a lifetime of 19 000 s produces CN with an ejection velocity of $v_d = 2.5$ km s^{-1} and a lifetime of 174 000 s. Fitting the observed CN profiles with variable velocities and lifetimes, the results indicate that the nature of the CN precursor in comet 21P/Giacobini–Zinner is still unclear, ruling out HCN as the only precursor and favouring a mixture of nitrogen compounds. Regarding C_2, the derived lifetimes are 35 000 and 62 000 s, if the parent and daughter velocities are fixed at ∼1 km s^{-1}. Gas production rates derived by means of the Vectorial modeling with the mentioned above lifetimes and velocities indicate that (i) the comet activity decreases with decreasing r_H (i.e. peak activity is not reached at the perihelion), and (ii) as already known, the comet is typically depleted in C_2 with a $\log \frac{Q_{C_2}}{Q_{CN}} \approx -0.4$. The azimuthally averaged surface brightness profiles of the continuum images are well fitted with $m \geq 1$ in a $\log B - \log \rho$ representation at projected radial distances (ρ) larger than 1000 km. The continuum light scattered from the dust in the coma of comet Giacobini–Zinner is redder than the Sun light on every date from Nov. 8 to 24, regardless the cometocentric distance. On Nov. 25, there is a sudden change in the dust color, being considerably bluer than the Sun, whereas on Dec. 7 and 8, the dust became much redder than it was before. These color variations do not seem to be related to sudden variations (relative minimum or maximum) in the cometary activity. The gas-to-dust mass ratio is ∼1, but affected by a large uncertainty (about a factor of 2) since the comet was not simultaneously imaged in the OH band, and the H_2O production rate has been considered from other measurements taken some weeks before ours.

Key words. comets: individual: 21P/Giacobini-Zinner – comets: general

1. Introduction

Comet 21P/Giacobini-Zinner (hereafter referred to as G–Z) is a short period comet (6.6 yr), with perihelion at a distance of 1.03 AU, belonging to the Jupiter-family and with a relatively stable orbit since it was discovered in 1900. However, it has been known for long that G–Z is an unusual comet in several aspects. Its molecular abundances had been noted as anomalous during previous apparitions, when C_2/CN, C_3/CN and NH/CN abundances were much lower than those measured in other comets (Bobrovnikoff 1927; Herbig 1976; Cochran & Barker 1987; Schleicher et al. 1987; Konno & Wickoff 1989; Beaver et al. 1990) and only slightly lower the CN/OH abundance. This fact seems to indicate that C_2, C_3 and NH are underabundant in the coma of G–Z. In their survey of 85 comets, A'Hearn et al. (1995) describe G–Z as the "prototypical carbon-depleted comet", with C_2 and C_3 abundances relative to H_2O ∼ 10 times lower than the values measured in most comets that define the "normal" cometary composition. A'Hearn et al. (1995) hypothesized that this depletion is associated with the formation

Send offprint requests to: L.-M. Lara, e-mail: lara@iaa.es region in the solar nebula, more concisely in a flat transNeptunian disk called the Edgeworth-Kuiper belt (EKb). On the other hand, the quasi–normality in the CN/OH abundance leaves open the possibility that other (excluding the C_2 and C_3 progenitors) carbon-bearing molecules in the nucleus may not be depleted.

This comet, during its 1985 apparition, also showed the peculiarity of peaking in gas production a full month before perihelion (McFadden et al. 1987), yet the visual light curve did not decline until after perihelion. Photometry in the 1–20 μm range by Hanner et al. (1992) confirmed that the visual light curve did not follow either the water production rate (which peaked ~30 days pre–perihelion) or the scattering and emitting cross section of dust in the inner coma. The shape of the light curve had varied from the 1979 to the 1985 apparition, implying that the location of active areas on the nucleus may have changed. Hanner et al. (1992) also concluded that the low abundance of C_2, C_3, NH and NH_2 is not associated with an unusually low dust/gas ratio.

At the time of the 1998 apparition, to our knowledge, G–Z was only observed by Weaver et al. (1999) during October 25–29, and by Mumma et al. (2000) during October 2–10 in the IR, and by Biver et al. (1999) in radio-wavelengths from Oct. 26 to 31. The IR observations by both groups were made using the same instrument CSHELL at the NASA Infrared Telescope Facility, Mauna Kea, Hawaii. Weaver et al. (1999) derived H_2O and CH_3OH production rates of ~(2–3) × 10^{28} s^{-1} and ~2.7 × 10^{26} s^{-1}, respectively. Emissions from C_2H_6, CO, HCN, C_2H_2 and H_2CO were also examined by Weaver et al. (1999) but were not clearly detected, it being possible only to set upper limits for their abundances relative to H_2O. From observations taken a few days before October 25–29, Mumma et al. (2000) were able to detect ethane and carbon monoxide for the first time in a Jupiter-family comet (probably originating in the EKb). The ethane production rate was $(7.0 \pm 1.5) \times 10^{25}$ s^{-1}, whereas carbon monoxide was produced at a rate of $(3.28 \pm 0.64) \times 10^{27}$. When compared with two comets probably originating in the giant-planets region (C/1996 B2 – Hyakutake – and C/1995 O1 – Hale-Bopp), the production rates and abundance ratios from G–Z may imply that ethane was depleted in precometary ices from the region of the solar nebula in which it formed in the EKb.

Charged Coupled Device (CCD) imaging and aperture photometry of G–Z were also conducted by Kiselev et al. (2000a,b) on November 20, 1998 and January 25, 1999. For both dates, there is an uncommon behaviour of polarization, i.e. the wavelength gradient of the polarization of its dust is negative. This effect is not caused by the presence of molecular emission in the pass band of the filter, but it may be due to either a large content of organic matter in its dust (Lebedinets 1991), or to an overabundance of large particles as compared to other comets (Hanner et al. 1992).

In this paper, we present pre- and post-perihelion CCD images of the gas (CN, C_2) and dust (green and red continua) coma of Comet 21P/Giacobini-Zinner, obtained with the 82 cm IAC–80 Telescope at Teide Observatory (Canary Islands, Spain) from November 8 to December 8, 1998. Assuming certain parent species, this data provide us with parent and daughter lifetimes (τ_p and τ_d), and the production rates Q for CN and C_2 from the best fit of the observed profiles with the Festou modeling (Festou 1981). The continuum images are used (i) to derive radial brightness profiles as a function of the projected distance to the nucleus, ρ, and to fit them with the law ρ^{-m}, and (ii) to obtain the dust production rate from the Afρ parameter. The gas and dust production rates enable us to compute C_2/CN and Afρ/CN (and thus the gas-to-dust mass ratio) abundances to better understand the nature of this comet in the framework of our and other previous and/or simultaneous observations.

2. Data acquisition and reduction

Comet G–Z was observed on nine photometric nights from November 8 to December 8, 1998, using the 82 cm IAC–80 Telescope at Teide Observatory (Canary Islands, Spain). CCD images were obtained using the Thomson 1024 × 1024 CCD (pixel size $0''.4325$, FOV ~ $7' \times 7'$) and the CN, C2, GC and RC narrow-band interference filters specifically designed to isolate continuum regions and some of the stronger emission bands in cometary spectra (see Farnham et al. 2000 for a detailed description of the filters). Several images of the comet, with the telescope tracking on the comet proper motion, were obtained each night using each filter. Details of the observations are presented in Table 1.

Several spectrophotometric standard stars and solar analogs from the list of Farnham et al. (2000) were observed each night at different airmasses to render the absolute calibration of the images. The air-mass coefficient, k_λ, was also determined for each filter, each night, using these data (see Table 2). The k_λ obtained for the narrow-band filters are coherent with the ones obtained for the broad-band filters usually installed at the IAC-80 telescope (see `http://www.iac.es/telescopes/ten.html`). Also, the day–to–day variations of the extinction coefficients so determined are similar to that observed with the broad-band filters and are mostly due to the variation of the amount of dust from the Sahara desert in the atmosphere of the observatory. As an example, on Nov. 8 there was a lot of dust over the observatory and the k_λ were larger than usual.

Images were reduced by making the overscan correction, and then using very high S/N ratio sky flat-fields obtained each night in order to correct pixel-to-pixel variations to below 1%. After that, all comet images were divided by their exposure times (in seconds) to normalize the image intensities to counts per second. The contribution of the sky was determined by computing the median of the pixels close to the border of the images, since the comet did not fill the field of view, and it was subtracted from each image. Then, the images were flux calibrated in the HB system, and the underlying continuum and gas contamination were removed following the procedure presented in Farnham et al. (2000).

To obtain the final images of the comet, the position of the comet optocenter in the calibrated images was determined by fitting a two-dimensional Gaussian to the inermost 20 pixels of the coma, all images were recentered and those taken with the same filter on each night were median combined. Examples

Table 1. Details of the observations.

Date (1998)	UT range	Images	Total Exp. time (s)	Filter	Air mass range	Δ (AU)	r_H (AU)	Phase (deg .)	Pixel scale (km)
Nov. 8	19:10–21:02	8	2400	CN	1.5–2.2	0.886	1.050	60.9	278
Nov. 8	19:22–20:45	4	1200	C2	1.4–2.0	0.886	1.050	60.9	
Nov. 8	19:33–20:56	4	1200	GC	1.5–2.1	0.886	1.050	60.9	
Nov. 8	19:28–20:51	4	1200	RC	1.5–2.1	0.886	1.050	60.9	
Nov. 10	19:18–20:58	9	2700	CN	1.4–2.2	0.879	1.046	61.3	276
Nov. 10	19:31–20:44	3	900	C2	1.5–2.0	0.879	1.046	61.3	
Nov. 10	19:04–20:21	4	1200	GC	1.4–1.8	0.879	1.046	61.3	
Nov. 10	19:37–20:50	3	900	RC	1.5–2.1	0.879	1.046	61.3	
Nov. 21	19:59–21:04	6	1800	CN	1.7–2.4	0.853	1.034	62.3	267
Nov. 21	20:16–20:47	2	600	C2	1.5–2.0	0.853	1.034	62.3	
Nov. 21	20:58–21:03	1	300	GC	2.3–2.3	0.853	1.034	62.3	
Nov. 21	20:22–20:53	2	600	RC	1.9–2.2	0.853	1.034	62.3	
Nov. 22	18:58–20:47	9	2700	CN	1.5–2.2	0.851	1.034	62.3	267
Nov. 22	19:19–20:27	3	900	C2	1.5–2.0	0.851	1.034	62.3	
Nov. 22	19:39–20:39	3	900	GC	1.6–2.1	0.851	1.034	62.3	
Nov. 22	19:26–20:33	3	900	RC	1.6–2.0	0.851	1.034	62.3	
Nov. 23	18:59–20:23	9	2700	CN	1.5–1.9	0.852	1.034	62.3	267
Nov. 23	19:19–20:27	3	900	C2	1.5–2.0	0.852	1.034	62.3	
Nov. 23	19:27–20:36	3	900	GC	1.6–2.1	0.852	1.034	62.3	
Nov. 23	19:30–20:47	3	900	RC	1.6–2.0	0.852	1.034	62.3	
Nov. 24	18:59–20:19	9	2700	CN	1.5–1.9	0.851	1.035	62.2	267
Nov. 24	19:16–20:30	3	900	C2	1.5–2.0	0.851	1.035	62.2	
Nov. 24	19:24–20:38	3	900	GC	1.6–2.1	0.851	1.035	62.2	
Nov. 24	19:30–20:33	3	900	RC	1.6–2.0	0.851	1.035	62.2	
Nov. 25	19:01–20:22	9	2700	CN	1.5–1.9	0.850	1.035	62.2	267
Nov. 25	19:18–20:28	3	900	C2	1.6–2.0	0.850	1.035	62.2	
Nov. 25	19:30–20:39	3	900	GC	1.6–2.1	0.850	1.035	62.2	
Nov. 25	19:24–20:33	3	900	RC	1.6–2.0	0.850	1.035	62.2	
Dec. 7	19:06–21:03	8	2400	CN	1.6–2.4	0.863	1.058	60.6	271
Dec. 7	19:38–20:30	3	900	C2	1.7–2.1	0.863	1.058	60.6	
Dec. 7	20:03–20:57	4	1200	GC	1.8–2.3	0.863	1.058	60.6	
Dec. 7	19:50–20:51	4	1200	RC	1.8–2.0	0.863	1.058	60.6	
Dec. 8	19:02–20:40	7	2100	CN	1.6–2.2	0.866	1.061	60.3	271
Dec. 8	19:30–20:46	4	1200	C2	1.7–2.2	0.866	1.061	60.3	
Dec. 8	19:55–20:19	3	900	GC	1.8–2.0	0.866	1.061	60.3	
Dec. 8	19:50–21:01	3	900	RC	1.7–2.4	0.866	1.061	60.3	

Images: number of images taken; Phase, r_H, Δ: the phase angle, heliocentric, and geocentric distances of the comet during the observations, respectively.

of the final images taken on Nov. 10 are shown in Fig. 1 in a logarithmic look–up table. We should note that, as we did not observe the comet in the C_3 band, it was impossible to remove any possible C_3 contamination in the *CN* band. In any case, this contamination should be very small (<10%) in the particular case of G–Z as it is a carbon-depleted comet.

3. Results

3.1. Spatial gas profiles

All the images were used to investigate the CN and C_2 profiles derived from an azimuthal average, leading to energy flux as a function of the projected radial distance, ρ. The conversion of the emission band fluxes into column densities was done with a constant g–factor for C_2 equal to 4.476×10^{-13} ergs s^{-1}mol^{-1} (A'Hearn et al. 1985) and g–factors for CN that were calculated for the heliocentric distances and heliocentric velocities of Comet 21P/Giacobini-Zinner from Nov. 8 to Dec. 8, 1998

Table 2. Air-mass coefficients.

Date (1998)	k_{CN}	k_{C2}	k_{GC}	k_{RC}
Nov. 8	0.50	0.25	0.27	0.12
Nov. 10	0.38	0.11	0.13	0.04
Nov. 21	0.47	0.12	0.13	0.05
Nov. 22	0.48	0.06	0.09	0.02
Nov. 23	0.35	0.06	0.08	0.01
Nov. 24	0.45	0.19	0.14	0.06
Nov. 25	0.44	0.08	0.09	0.01
Dec. 7	0.38	0.16	0.11	0.06
Dec. 8	0.33	0.09	0.12	0.02

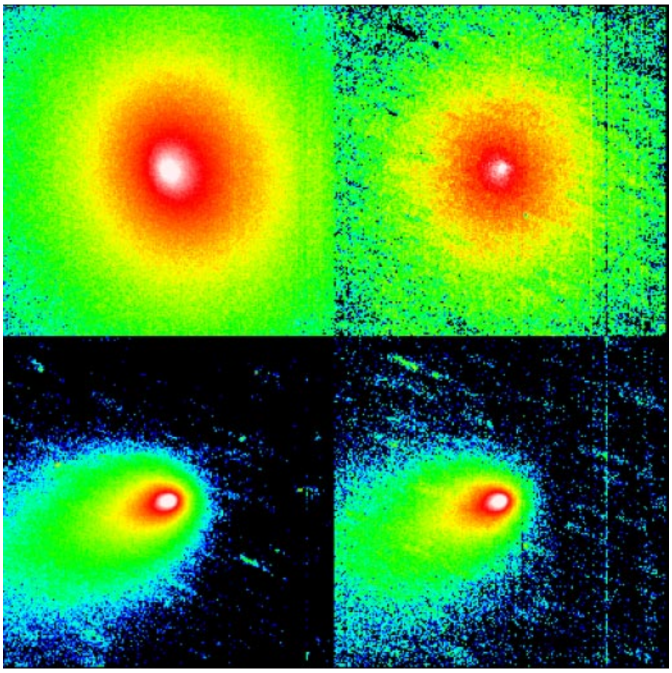

Fig. 1. Series of bias and flat–field corrected images taken on Nov. 10, 1998. After that images were flux calibrated in the HB system, and the underlying continuum and gas contamination were removed. From left to right and top to bottom: CN, C_2, red continuum, and green continuum. The scale is 173.″43 × 173.″43 (i.e. 111 478 × 111 478 km at the comet distance) for all of them. North is down and East to the left. The CN image shows a clear elongation in the direction perpendicular to the Sun position, as projected on the plane of the sky. C_2, green and red continuum images show the typical spherical gas coma, and the dust coma and tail, respectively.

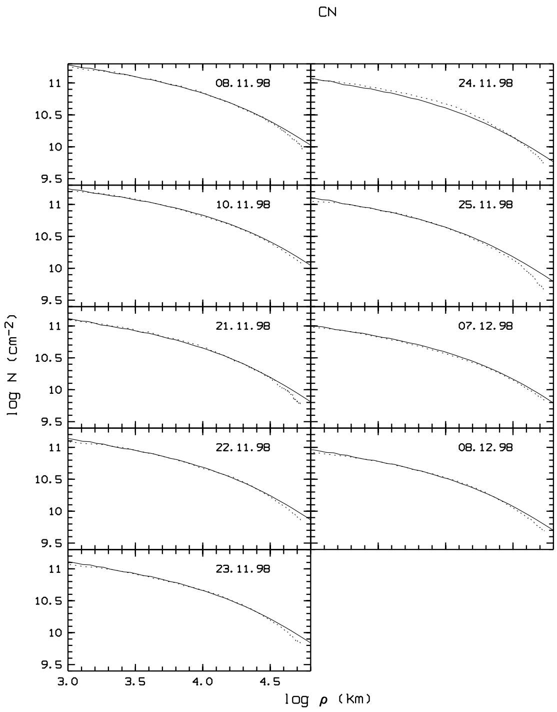

Fig. 2. Azimuthally averaged CN column density profiles of Comet 21P/Giacobini–Zinner (dots). The solid lines represent the results obtained by means of the Vectorial model with fixed $v_p = 0.85 \times r_H^{-0.5}$ and $v_d = 1.19$ km s^{-1} whereas (τ_p, τ_d) and Q_{CN} are the best fit parameters listed in Table 3 under these velocities conditions.

from the set of values given by Schleicher (1983), and are listed in Table 3.

The azimuthally averaged CN and C_2 spatial profiles are presented in Figs. 2 and 3, respectively, together with the theoretical profiles best resembling the observed ones. These theoretical profiles were obtained by means of the Festou modeling (Festou 1981), where parent and daughter and lifetimes (τ_p, τ_d) at $r_H = 1$ AU, as well as production rates, Q, were derived as follows.

Assuming that HCN might be the CN precursor, we fix $v_p = 0.85 \times r_H^{-0.5}$ (Biver et al. 1999b, 2000) and $v_d = 1.19$ km s^{-1} (Bockelée–Morvan & Crovisier 1985). To derive the (τ_p, τ_d) that best resemble the shape of the observed profiles, we constructed theoretical radial profiles with an arbitrary (however approximated) gas production rate with lifetimes spanning the reported values, i.e. τ_p ranging from 1.6×10^4 s to 6.6×10^4 s, whereas τ_d covered the $(1.5–4.0) \times 10^5$ s. Once the theoretical profile was computed, we compared it with the observed profile by dividing both profiles. We selected the profiles computed with (τ_p, τ_d) giving rise to those theoretical profiles whose standard deviation of the quotient calculated at distances $3 < \log\rho < 4.64$ (i.e. between 1×10^3 and 3.2×10^4 km not to hit the sky) was lower than 3×10^{-3}. All of the (τ_p, τ_d) better fitting the observed profiles for every date (i.e. parameters producing quotient images with the lowest standard deviation, in some cases as low as 3.6×10^{-4}) were then averaged to produce the values listed in Table 3. These daily averages have standard deviations ≤17% for τ_p, and ≤24% for τ_d. The gas production rates were obtained once the lifetimes were derived and the values are also presented in Table 3. As the CN precursor is not clearly known, according to Krasnopolsky (1991) a mixture of C_4N_2 and HC_3N expanding at 1 km s^{-1}, might give rise to CN with an ejection velocity of 2.5 km s^{-1}. By considering these velocities, the procedure to derive lifetimes was the same as outlined above and the best theoretical profiles were obtained with the lifetimes listed in parenthesis in Table 3 where the uncertainties in both lifetimes are of the same order as in the previous case. Differences among individual τ_p and τ_d are not outstandingly large. As a final test, we additionally allowed (v_p, v_d) to vary from 0.6 to 1.2 km s^{-1} and 1.0 to 3.0 km s^{-1}, respectively. Theoretical profiles were obtained for every combination of (v_p, v_d, τ_p, τ_d) and then compared to the observed ones following the same criteria as previously mentioned. In this case, the values of (v_p, v_d, τ_p, τ_d) providing the best daily fits are affected by an uncertainty of ≤25%. Averaging these pre– and post–perihelion values, we obtain $v_p = (0.84 \pm 0.06)$ km s^{-1}, $v_d = (1.38 \pm 0.37)$ km s^{-1}, $\tau_p = (19.5 \pm 2.2) \times 10^3$ s and $\tau_d = (2.68 \pm 0.18) \times 10^5$ s, where the errors represent the standard deviation of the sample. It should be noted that the parent and daughter velocities so derived are merely indicative. The profiles are very sensitive to the parent and daughter scale lengths, and therefore to the two products $v_p\tau_p$ and $v_d\tau_d$ of the Haser-equivalent parameters (Combi & Delsemme 1980a,b) or to more complex combinations of the physical parameters.

Table 3. CN $g-$factors, τ_p, τ_d and Q derived from the best fits to the observed profile by using the Festou modeling assuming that $v_p = 0.85 \times r_H^{-0.5}$ and $v_d = 1.19$ km s^{-1} or that $v_p = 1$ km s^{-1} and $v_d = 2.5$ km s^{-1} (values in parenthesis). CN production rate from Haser modeling assuming standard l_p and l_d. Measurement of the dust-to-gas ratio by means of log $\frac{Af\rho}{Q_{CN}}$.

Date 1998	g–factor[a] 10^{-13}	τ_p 10^4 s	τ_d 10^5 s	Q_{Fes} 10^{25} s^{-1}	Q_{Has} 10^{25} s^{-1}	[b]log $\frac{Af\rho}{Q_{CN}}$ cm s
Nov. 8	3.16	1.91 (1.97)	2.69 (1.98)	4.72 (9.27)	4.44	−22.82
Nov. 10	3.04	2.45 (2.21)	2.23 (2.08)	5.20 (9.59)	4.34	−22.82
Nov. 21	2.36	1.74 (1.71)	2.65 (1.34)	2.95 (5.95)	2.87	−22.83
Nov. 22	2.42	1.87 (1.94)	2.73 (1.86)	3.30 (6.51)	3.10	−22.84
Nov. 23	2.50	1.87 (1.99)	2.74 (1.70)	3.09 (6.20)	2.93	−22.98
Nov. 24	2.56	1.69 (1.80)	2.58 (1.68)	2.86 (5.70)	2.82	−22.87
Nov. 25	2.70	1.71 (1.63)	2.63 (1.33)	2.66 (5.34)	2.67	−22.94
Dec. 7	4.31	2.31 (2.08)	2.16 (2.04)	2.92 (5.40)	2.45	−23.06
Dec. 8	4.35	1.83 (1.81)	2.66 (1.65)	2.23 (4.43)	2.14	−23.03
Average[c]		1.93 ± 0.27	2.56 ± 0.21	(2.86 ± 0.34)[e]	(2.71 ± 0.32)[e]	−22.91 ± 0.09
Average[d]		1.90 ± 0.18	1.74 ± 0.28	(5.64 ± 0.68)[e]		

[a] erg s^{-1} mol^{-1}.
[b] CN production rate derived from the Haser modeling, and $Af\rho$ obtained by integrating the green continuum flux in a circular aperture of $\rho < 10\,000$ km.
[c] Pre- and post-perihelion averaged values in the case of $v_p = 0.85 \times r_H^{-0.5}$ and $v_d = 1.19$ km s^{-1}.
[d] Pre- and post-perihelion averaged values in the case of $v_p = 1$ km s^{-1} and $v_d = 2.5$ km s^{-1}.
[e] Averaged values by considering postperihelion production rates.

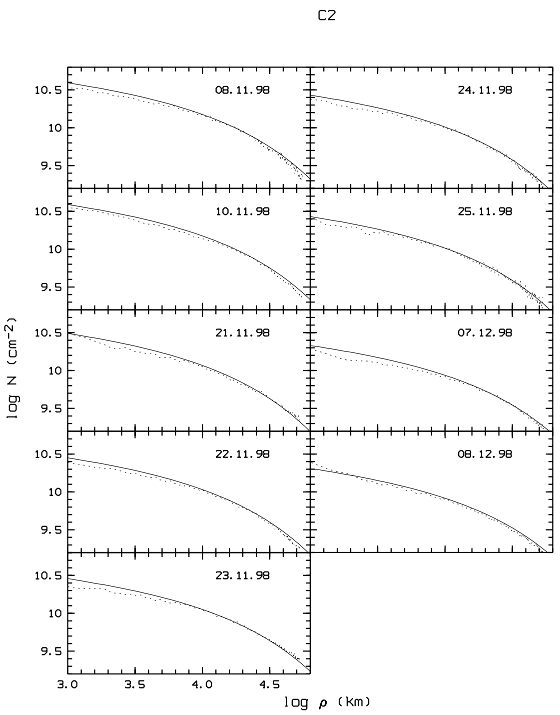

Fig. 3. Azimuthally averaged C2 column density profiles of Comet 21P/Giacobini–Zinner (dots). The solid lines represent the results obtained by means of the Vectorial model with parent and daughter lifetimes and Q_{C_2} listed in Table 4.

Theoretical predictions of the photodissociation time scales for many cometary species under solar irradiance have been provided by Huebner & Link (1999) and Huebner et al. (1992). Solar photo rate coefficients and excess energies for dissociation and ionization are calculated both for low and high solar activity. According to Huebner & Link (1999), the lifetimes for HCN and CN at 1 AU amount to 7.94×10^4 s and 3.15×10^5 s at low solar activity, and to 3.19×10^4 s and 1.34×10^5 s at high solar activity. Bockelée–Morvan & Crovisier (1985) reported the HCN photodissociation rate of the order of 1.5×10^{-5} s^{-1}, i.e. lifetime $\sim 6.7 \times 10^4$ s. A more precise HCN lifetime, corresponding to the solar activity of Nov.–Dec. 1998, may be estimated as 4.8×10^4 s (Crovisier 2002, private communication). From our analysis of the CN profiles, the parent lifetime we obtain, $(1.93 \pm 0.27) \times 10^4$ s, is lower than that expected for HCN as the sole precursor of CN. On the other hand, the deduced CN lifetime, $(2.56 \pm 0.21) \times 10^5$ s, agrees well with theoretical determinations for a moderate-to-high solar activity. For a mixture of nitrogen compounds (for example C_4N_2 and HC_3N) as the CN parent species, the obtained $\tau_p = (1.90 \pm 0.18) \times 10^4$ s approaches the theoretical values of cyanoacetylene $(1.4 - 2.6) \times 10^4$ s and, to a lesser extent, of dicyanogen, $(0.74 - 2) \times 10^4$ s. A mixture of nitrogen compounds, richer in HC_3N than in C_4N_2, not ruling out HCN, could be considered as the CN precursor in G–Z.

The results of the problem of four parameter (velocities and lifetimes) fits do not provide a firm constraint to the "determination" of the CN parent species. Although v_p favours HCN (an expansion velocity 10% lower than that deduced for Comet Hyakutake and Comet Lee can be expected, Biver et al. 1999b, 2000, 2002, private communication), the deduced parent lifetime is too short compared to 4.8×10^4 s as deduced for the solar activity of Nov.–Dec. 1998 (Crovisier 2002, private communication). Similarly, a CN ejection velocity of (1.38 ± 0.37) km s^{-1} might rule out HCN as its only precursor (note that the uncertainty is large and 1.19 km s^{-1} is within the v_d derived values), pointing to a mixture of nitrogen compounds (hydrogen cyanide, cyanoacetylene, dicyanogen) as cyanogen parent species.

Given that CN production rates can considerably vary as a function of parent and daughter velocities and lifetimes (see Table 3), we have also used the Haser modeling (Haser 1957) to fit the observed column density profiles in order to consistently compare our results with those published in the 85 comet survey by A'Hearn et al. (1995), or with G–Z specific observations (Schleicher et al. 1987; Beaver et al. 1990; Churyumov et al. 1991; Landaberry et al. 1991; Singh et al. 1997; and Ellis & Neff 2000). Although the Haser formalism is physically unrealistic, it is an empirical description that can serve as a basis of comparison of gas production and distribution in different comets observed under quite different circumstances of heliocentric and geocentric distances and aperture sizes. The Haser model scale lengths are not meant to be true molecular scale lengths, but rather values that best fit the observed spatial distribution when using this formalism. The resulting production rates can be compared with those derived from the more physically relevant production as obtained from the Vectorial modeling (Festou 1981). Thus, we use the Haser scalelength equal to 1.3×10^4 and 2.1×10^5 km, for CN parent and CN itself, respectively, with a r_H^2 variation (A'Hearn et al. 1995; Randall et al. 1992). Velocities are held constant at 1 km s^{-1}. The best CN production rates fitting the observed profiles are also included in Table 3. Differences in Q from both models can be as high as a factor of 2. Fits to observed profiles by means of this formalism are as good as those presented in Fig. 2 with the Vectorial modeling (Festou 1981).

Regarding C_2, we followed the same approach as for CN. Parent and daughter lifetimes for the Vectorial modeling ranged from 30 000 to 45 000 s, and from 40 000 to 100 000 s, respectively. Velocities were held constant and equal to 1 km s^{-1} (values proven to be a reasonable approximation from the analysis of the coma distortions caused by radiation pressure acceleration, Schulz et al. 1993). It is well known that C_2 does not seem to be produced by a single photolytic step, the observed profiles being flatter than the ones produced by the vectorial or Haser model in the inner coma. By taking v_p of the same order as CN (i.e. $v_p \approx 0.83$ km s^{-1}), the C_2 parent lifetime has to be larger than 10^5 s to obtain a reasonable fit of the C_2 column density at distances shorter than 5000 km. After computing theoretical profiles for every combination of τ_p and τ_d and comparing them with the observed ones, we averaged those pairs (τ_p, τ_d) satisfying the criterium previously stated. The resulting lifetimes are presented in Table 4 together with the gas production rates computed by means of the Vectorial modeling. Bearing in mind that the C_2 parent remains unknown (halo of large icy particles, three-step grandparent–parent–daughter, and CHON grain halo scenarios have been claimed), the deduced lifetimes are of the same order as determinations for other comets such as Comet Wilson (1987VII) (Schulz et al. 1993). The Haser formalism has also provided us with C_2 production rates by considering $l_p = 2.2 \times 10^4$ km and $l_d = 6.6 \times 10^4$ km with a r_H^2 dependence, $v_p = v_d = 1$ km s^{-1}. As it is the case for CN, gas production rates derived from the Vectorial and from the Haser modeling also differ by as much as ~43%. The last column in Table 4 lists the log of the CN/C_2 abundance by considering gas production rates computed from the Haser modeling for both species.

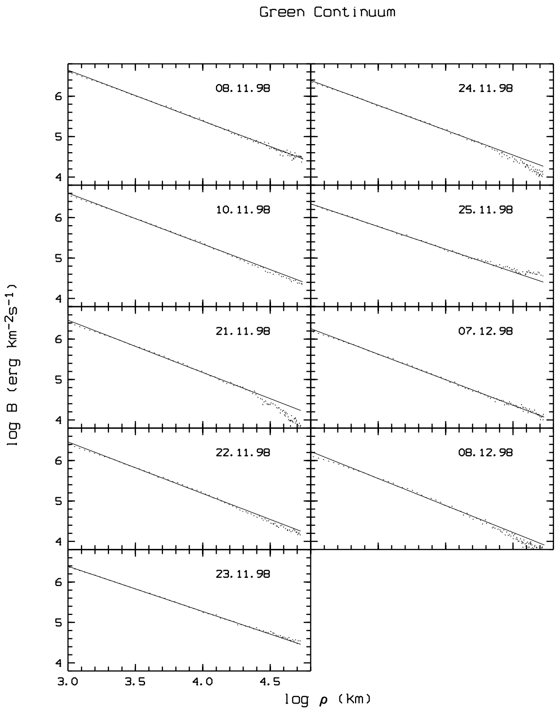

Fig. 4. Brightness profiles of Comet 21P/Giacobini-Zinner in the green continuum. The profiles were obtained from azimuthal averaging of the images. The surface brightness, B, is plotted against the projected radius, ρ, in double logarithmic representation. Dots represent the observed profiles and the solid lines are the best fits verifying $\frac{d(\log B)}{d(\log \rho)} = -m$ starting at $\log \rho \geq 3$, with slopes listed in Table 5.

3.2. Dust profiles

The comet was imaged in two different continuum regions centered at 5259 Å and 7133 Å, green and red, respectively. The flux calibrated continuum profiles were multiplied by $4\pi\Delta^2$ and r_H^2 and normalized to a unit area of 1 km^2 at the position of the comet. This leads to a surface brightness in erg s^{-1} km^{-2}, which is independent of the geocentric distance Δ and normalized to the solar flux at $r_H = 1$ AU (see Schulz et al. 1994). It therefore allows a direct comparison of the day–to–day variations in the continuum images, and thus in the continuum profiles.

Figures 4 and 5 show the brightness profiles derived from an azimuthal average of the continuum images in a log–log representation. The profiles exhibit a normal radially expanding dust coma and they can be well fitted with a ρ^{-m} law with $0.82 < m < 1.33$ (see Table 5) for $3 < \log\rho < 4.4$, i.e. between 1×10^3 km and 2.5×10^4 km projected radial distance from the nucleus. The effect of radiation pressure is clearly visible leading to slopes that are always somewhat higher than 1. This is consistent with a steady state coma for a constant dust production rate and long-lived grains expanding radially outwards, where the spatial number density should decrease as r^{-2}, r being the nucleocentric radial distance. Consequently, the projected surface brightness would decrease as ρ^{-1}.

Estimates of the dust production in comets are usually made by means of the parameter $A(\theta)f\rho$ (A'Hearn et al. 1984). $A(\theta)$ is the Bond albedo for the particular scattering angle, θ,

Table 4. τ_p, τ_d and Q for C_2 derived from the best fits to the observed profile by using the Vectorial modeling. C_2 production rate from Haser modeling assuming standard l_p and l_d. Measurement of the C_2 to CN ratio.

Date 1998	τ_p 10^3 s	τ_d 10^3 s	Q_{Fes} 10^{25} s^{-1}	Q_{Has} 10^{25} s^{-1}	$^a\log \frac{Q_{C_2}}{Q_{CN}}$
Nov. 8	33.5	56.6	2.08	1.45	−0.48
Nov. 10	33.6	61.5	2.02	1.44	−0.48
Nov. 21	32.5	57.9	1.56	1.13	−0.40
Nov. 22	34.0	58.8	1.47	1.04	−0.47
Nov. 23	36.0	67.0	1.54	1.11	−0.42
Nov. 24	34.4	60.1	1.41	1.00	−0.45
Nov. 25	33.6	57.1	1.40	1.00	−0.43
Dec. 7	37.6	70.4	1.23	0.88	−0.44
Dec. 8	37.6	70.4	1.18	0.84	−0.41
Average	34.7 ± 1.9	62.2 ± 5.6	$(1.44 \pm 0.12)^b$	$(1.00 \pm 0.11)^b$	−0.44 ± 0.03

[a] CN and C_2 Production rates derived from the Haser formalism. [b] Post-perihelion Q_{C_2} average.

Table 5. Linear fits to the brightness continuum profiles. Dust production rate by means of the parameter $Af\rho$ and color of the cometary grains measured as the reddening of the dust.

	Green Continuum			Red Continuum			Reddening	
Date	m	$Af\rho$ (cm)		m	$Af\rho$ (cm)		% / 1000 Å	
1998		10^4 km	1.5×10^4 km		10^4 km	1.5×10^4 km	10^4 km	1.5×10^4 km
Nov. 8	1.26	670	822	1.25	830	1010	12.8	12.2
Nov. 10	1.26	656	797	1.24	644	806	−0.9	6.7
Nov. 21	1.29	420	544	1.18	567	649	18.7	10.3
Nov. 22	1.27	444	548	1.22	564	669	14.5	11.8
Nov. 23	1.12	305	354	1.00	388	401	14.6	7.1
Nov. 24	1.23	380	462	1.21	440	522	8.4	7.1
Nov. 25	1.12	309	353	0.82	223	206	−14.9	−22.0
Dec. 7	1.26	209	273	1.19	300	363	23.3	17.4
Dec. 8	1.33	197	264	1.21	302	367	28.5	20.6

of the observations, f is the filling factor of the grains in the field of view (number of grains per unit area times their mean cross-section divided by the area of the field of view), and ρ is the radius of the assumed circular field of view. This parameter assumes that physical characteristics of the dust grains remain unchanged as they move outward and that the column of grains is optically thin. Table 5 also contains the values for $A(\theta)f\rho$ computed in circular apertures of 1×10^4 km and 1.5×10^4 km radius.

A relative determination of the gas-to-dust ratio for G–Z can be made by computing the ratio of the OH production rate to $Af\rho$. If CN is produced in constant proportion to OH (Schleicher et al. 1987), the Q(CN)/$Af\rho$ quantity is proportional to Q(OH)/$Af\rho$ and, therefore, the gas-to-dust mass ratio can be determined. Since G–Z was not imaged with the OH narrowband interference filter, we have used the CN observations and the mean ratio of OH to CN, log $(Q(\mathrm{OH})/Q(\mathrm{CN})) = 2.5$ (A'Hearn et al. 1995), to derive the OH production rate. Typical values for log $(Q(\mathrm{OH})/Q(\mathrm{CN}))$ range from 2.83 to 2.17, which implies that the OH derived from this expression can reasonably be as much as 2 times smaller or larger than the actual value. In line with A'Hearn et al. (1995), the gas-to-dust mass ratio can be evaluated by

$$\log\left(\frac{M_{\mathrm{gas}}}{M_{\mathrm{dust}}}\right) = \log[Q(\mathrm{OH})/Af\rho] - 25.4. \quad (1)$$

According to this expression and using the Q_{CN} obtained with the Haser model (see Table 3), we computed a mean gas-to-dust mass ratio of ∼1.02 during our observations (with an error of a factor of ∼2, introduced by the approximate Q_{OH}). The $\log\left(\frac{Af\rho}{Q_{CN}}\right)$ on every date is also listed in Table 3. Note that these ratios can be directly related to the log of the gas-to-dust mass ratio by simply adding 22.9.

Since the comet was imaged in two continuum filters, we used the calibrated images to determine the average dust color and to search for spatial variations. We first computed the color two-dimensionally according to

$$color = -2.5\ \log\left(\frac{F_c(\lambda)}{F_c(\lambda')}\right), \quad (2)$$

being F_c the cometary flux in erg cm^{-2} s^{-1} at two different wavelengths, λ and λ', with $\lambda' > \lambda$. In our case, λ and λ' correspond to the central wavelengths of the GC and RC continuum filters, i.e. $\lambda_c = 525.9$ and $\lambda'_c = 713.3$ nm, respectively. The resulting two dimensional images show no clear features. The color or reddening of the dust can be also computed in terms of $Af\rho$:

$$reddening = \frac{1}{Af\rho}\frac{(Af\rho)' - (Af\rho)}{\lambda' - \lambda}, \quad (3)$$

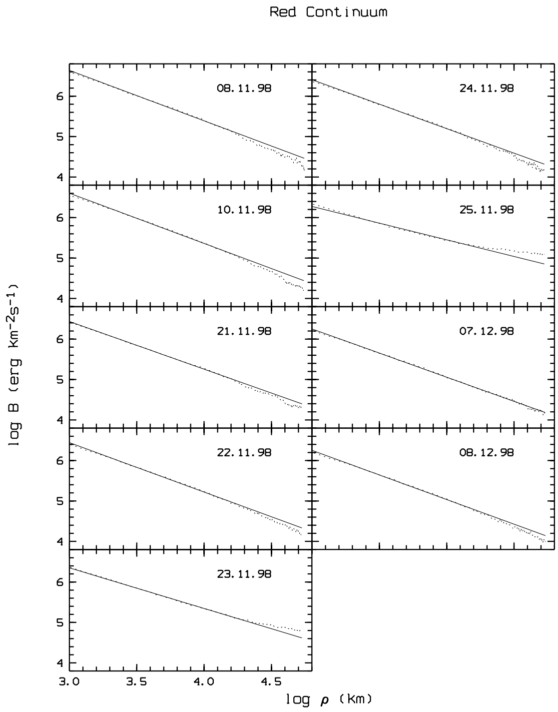

Fig. 5. Brightness profiles of Comet 21P/Giacobini-Zinner in the reed continuum. The profiles were obtained from azimuthal averaging of the images. The surface brightness, B, is plotted against the projected radius, ρ, in double logarithmic representation. Dots represent the observed profiles and the solid lines are the best fits verifying $\frac{d(\log\ B)}{d(\log\ \rho)} = -m$ starting at log $\rho \geq 3$, with slopes listed in Table 5.

where $(Af\rho)$ is computed at wavelengths $\lambda = 525.9$ nm and $\lambda' = 713.3$ nm.

Values for $Af\rho$ have been considered for two different circular apertures (i.e. 1×10^4 and 1.5×10^4 km) and the average color of the dust in regions $\rho \leq 1\times10^4$ km and $\rho \leq 1.5\times10^4$ km is shown in Table 5.

4. Discussion

To our knowledge, no other optical observations of G–Z during the 1998 passage were made, or have been published so far. Therefore, our results can be only compared to those obtained during previous approaches of the comet to the Sun, or to global results of the gas and dust behaviour in a Jupiter-family comet at similar heliocentric distances.

As already noted by several authors (Schleicher et al. 1987; Beaver et al. 1990; Churyumov et al. 1991; Landaberry et al. 1991; Singh et al. 1997; and Ellis & Neff 2000), it is clear that the gas production rate seems not to peak at the perihelion (Nov. 21) but some time before (see Tables 3 and 4) . Although our observations all take place in the vicinity of the perihelion date, this trend is clear and the comet activity (gas and dust) steadily decreases from Nov. 8 to Dec. 8 with day-to-day variations of ≤20%. As known from previous passages of the comet and as mentioned in the introduction, the C_2 abundance, relative to CN (and to OH), is unusually low as compared with that normally seen in comets.

During the 1985 apparition, observations by Schleicher et al. (1987) gave rise to log $\frac{Q_{C_2}}{Q_{CN}} = -0.94$ as the average value from pre- and post-perihelion observations (r_H = 1.507 AU on June 15 to R_H = 1.457 AU, Nov. 20, 1985, perihelion date for the 1985 approach was on Sept 9). Beaver et al. (1990), from observations on June and on Sept 1985, reported a C_2 to CN mean relative abundance of 0.11, that is, log $\frac{Q_{C_2}}{Q_{CN}} \sim -0.96$. On the other hand, Landaberry et al. (1991) derived a slightly higher value of –0.52 (assuming a gas expansion velocity of 1 km s^{-1} for both species) from post–perihelion observations on Oct. 10, 1985 when the comet was at r_H = 1.17 AU. Our results are closer to those of Landaberry et al. (1991) (−0.44 ± 0.03 vs. −0.52) which could be expectable since our and Landaberry et al.'s observations were made when the comet was closer to perihelion. From the survey of 85 comets by A'Hearn et al. (1995), G–Z was classified as a C_2 depleted comet with log $\frac{Q_{C_2}}{Q_{CN}} = -0.67$. The C_2 depletion in the coma of G–Z has not yet been explained as the detailed chemistry giving rise to C_2 is still not clear (note that the inner log N vs. log ρ profiles have been repeatedly reported to be too flat to be produced by a single parent species and in single photodissociation step). Comparing the available C_2H_6 detections in Oort-cloud comets (i.e. in comets C/1996 B2, C/1995 O1 and C/1999 H1) and Jupiter family comets (21P/Giacobini–Zinner), G–Z appears to be also depleted in C_2H_6 compared to comets Hyakutake, Hale–Bopp and Lee which are "typical" comets in terms of C_2 abundance.

The detection of ethane in G–Z (first detection in a Jupiter-family comet) by Mumma et al. (2000) allowed them to establish an ethane production rate of $(7.0 \pm 1.5) \times 10^{25}$ s^{-1} at r_H = 1.25 AU. If ethane is the only precursor of C_2, and $Q_{C_2H_6}$ scales as $r_H^{-2.7}$, the quantum yield of the process $C_2H_6 \rightarrow C_2$ + products is ≥0.09, i.e. ∼10 molecules of ethane are required to form one C_2 molecule. From the same observations, a line of H_2O ($1_{11} - 1^{10}$ in the $\nu_3 - \nu_2$ hot band, Dello Russo et al. 2000) should have appeared near the clearly detected $R1$ line of CO. No strong line was seen and the excess of flux at the proper frequency (2151.26 cm^{-1}) allowed Mumma et al. to establish an upper limit for the water production rate of $(3.2\pm1.7)\times10^{28}$ s^{-1} at r_H = 1.25 AU (October 2-10, 1998). Scaling this production rate by r_H^k with $k = -2.7$ (A'Hearn et al. 1995) to ∼1.04 AU at the time of our observations, the water production rate could have been $\sim 5.3 \times 10^{28}$ s^{-1}. Therefore, the production rate of C_2H_6 relative to that of H_2O is much higher than the C_2 one (2.2×10^{-2} vs. 2.0×10^{-4}) assuming that the variations of the gas production rates as a function of heliocentric distance are the same for both species. At this point, we note that Weaver et al. (1999) could not detect any ethane emission in the coma of G–Z from infrared spectra taken two weeks after Mumma et al.'s observations, only an upper limit of 1.6×10^{25} s^{-1} could be set. This upper limit to the ethane production rate together with a water production rate in the order of $(2–3) \times 10^{28}$ (Weaver et al. 1999) adequately scaled to $r_H \sim 1.04$ AU (i.e. 2.95×10^{28} s^{-1}) provides $C_2H_6/H_2O \leq 0.05 - 0.08\%$, in the same order as the C_2/H_2O derived in this work (0.04%) when using $Q_{C_2} = 1.1 \times 10^{25}$ s^{-1} from Table 4.

Contrary to the C_2 depletion in G–Z, CN seems to have a "quasi–normal" abundance relative to H_2O. The CN production rate from Nov. 8 to Dec. 8, 1998 slightly decreases with decreasing r_H (that is, when the comet approaches perihelion) with negligible day-to-day variations (~15%). The ratio of CN to OH production rates is $\sim 7\times10^{-4}$ assuming that the water production rate at $r_H = 1.1$ AU is $(5.6\pm0.4)\times10^{28}$ s^{-1} (Biver et al. 1999a) conveniently scaled by $r_H^{-2.7}$ to ~1.04 AU. On the other hand, if we consider the H_2O production rate given by Weaver et al. (1999) from IR observations, this ratio increases to 0.15%. These two values bracket a value of log $\frac{Q_{CN}}{Q_{OH}}$ between −3.15 and −2.82, which is more characteristic of "depleted" comets (see Table VI in A'Hearn et al. 1995) as G–Z indeed is, than of a normal comet. Comparing this ratio to that obtained from previous passages of the comet, Schleicher et al. (1987), from observations at similar r_H as ours (from 1.053 to 1.043 AU), derived a CN production rate of $7.2\times10^{25} \le Q_{CN} \le 3.63\times10^{25}$ s^{-1} by means of the Haser model. The values presented here are similar to these ones, whereas the relative abundance of CN to OH during the 1985 passage (0.2%) can be considered similar to the one derived in this work during the 1998 approach (0.15–0.07%). These differences, if any, given the uncertainties in the determination of OH production, can be attributed to different behaviour of the comet and/or to different scale lengths in the Haser modeling, and/or to different production rates of H_2O directly measured in the IR or indirectly (OH in radio wavelengths or in the UV).

During their IR investigation of volatiles in the coma of G–Z, Weaver et al. (1999) were not able to detect HCN. This non-detection allowed them to set an upper limit for the HCN production rate of 5.4×10^{25} s^{-1}, later confirmed by Biver et al. (1999a) ($Q_{HCN} \sim 3\times10^{25}$ s^{-1}), and a quotient of the HCN to H_2O abundance of 0.05 to 0.07% at $r_H \sim 1.1$ AU below the normal abundances of 0.08–0.25% (Biver et al. 2002). It is interesting to note that this HCN/H_2O is very similar to the CN/H_2O(=0.11% to 0.22%) that we report from our CN measurements and available water measurement, either from IR (Weaver et al. 1999) or OH radio observations (Biver et al. 1999a). At first sight, this result seems to indicate that CN can be solely produced by HCN, however the required $\tau_p(\sim2\times10^4$ s) to fit the CN column density profiles by means of the Vectorial model is low when compared with determinations by Bockelée-Morvan & Crovisier (1985) or by Huebner & Link (1999). The nowadays available information is not enough to rule out other CN parent, species such as C_2N_2 (Festou et al. 1998; Komitov & Bonev 1999), C_4N_2+HC_3N (Krasnopolsky 1991) and/or evaporation from the dust grains.

Our dust analysis of the surface brightness profiles has shown that most profiles can be fit by the law log $B \sim -m$ log ρ with $1 < m \le 1.33$ (except the red continuum profile on Nov. 25 which shows a slightly flatter profile) in contradiction with previous analysis of the G–Z brightness profiles by Jewitt & Meech (1987). These authors indicated that the log B profile vs. log ρ for G–Z did not strictly follow the law log $B \sim -m$ log ρ with $1 \le m \le 3/2$ at distances larger than 10″ from the nucleus (~7500 km or log $\rho = 2.87$ in our case), and the negative curvature dm/d log$\rho < 0$ could be indicative of variations in the strength of the nucleus source on time scales comparable to the grain flight time. In fact, the activity of G–Z did vary during our observations, but the derived continuum profiles do not exhibit slopes higher than 3/2 at distances from the nucleus larger than 10″ (log $\rho \sim 2.9$). The dust production rate, either derived from the green or the red continuum filter, decreases from Nov. 8 to Dec. 8, regardless of the approach of the comet to the Sun.

The polarization of the scattered light of the dust particles in G–Z has an unusual behaviour. Contrary to all other comets, the wavelength gradient of the polarization of the continuum is negative. Kiselev et al. (2000a,b) have attributed this effect to a high abundance of organic matter in its dust and/or to an overabundance of large particles, also supported by the weak 10 μm silicate feature detected by Hanner et al. (1992). However, comets with low abundance of submicron silicate grains have a low degree of polarization (10–15%) for both the blue and the red domain of the spectrum at large phase angles, this not being the case for G–Z. Due to this, Kiselev et al. (2000a,b) favour the idea that the dust particles in G–Z have an overabundance of organic matter. Furthermore, an abundance of large particles in the coma may also produce a redder colour as is computed from our continuum images at $\rho \le 10\,000$ km. The reddening of the dust ranges from a common 13%/1000 Å (in agreement with the ~15% reported by Schleicher et al. 1987) to a high value of 29%/1000 Å which could be indicative of an overabundance of large grains in the dust coma of G–Z after the perihelion (Dec. 7 and 8, 1998).

Although the general behaviour of the dust color is to be redder than the Sun, there are two dates when this trend was not followed. On Nov. 10, the dust was neutral (Sun color) and on Nov. 25 it was much bluer than the Sun. On the latter date, the dust production rate decreased by a 20% (if measured in the green continuum) and by a 50% (if measured in the red continuum) with respect to the previous day, and this variation had no clear counterpart in the gas activity since it was steadily decreasing from Nov. 8 to Dec. 8. Previous observations by Singh et al. (1997) also noticed a change of color (from red to blue relative to the Sun) of grains during a 24 h period in G–Z together with a Q_{CN} decrease of 25%. However, as these authors only observed the comet on Oct. 15 and 16, 1985, we cannot conclude that this sudden blueing of the dust was due to a noticeable variation in the cometary activity.

Regarding the gas-to-dust mass ratio, it can vary largely depending on the water production rate we use (from 1.02 to 3.6, lower than and similar to previous passages, respectively). Schleicher et al. (1987) determined a relative gas-to-dust ratio by simply dividing the OH production rate (s^{-1}) and $Af\rho$ (cm) which resulted in a value of 1×10^{26} s^{-1} cm^{-1}. By applying Eq. (1), the gas-to-mass ratio is ~4. Singh et al. (1997) concluded that the dust-to-gas ratio was always less than unity (that is, gas-to-dust ratio > 1) during Oct. 15–16, 1985. In Table III in A'Hearn et al. (1995), log $\frac{Af\rho}{Q_{OH}}$ is –25.94, which means a gas-to-dust mass ratio of ~3.5. Mumma et al.'s (2000) determination for the water production rate at $r_H = 1.25$ AU adequately scaled to ~1.04 AU, at the time of our observations, allows us to derive a mean gas-to-dust mass ratio of 3.6 from Nov. 8 to Dec. 8, 1998. Let us note that this value might be affected by some errors since the gas production can substantially vary from one comet to another and the expression $Q \sim r_{\rm H}^{-2.7}$ may be inaccurate for G–Z. In fact, if we assume this water production rate as valid, this would mean that OH is produced at a rate of 3.51×10^{28} s^{-1} (relatively higher than the maximum reported measurement of 3.23×10^{28} s^{-1} in A'Hearn et al. 1995), meaning log $(Q(\mathrm{OH})/Q(\mathrm{CN})) = 3.1$, larger than the typical 2.83–2.17 given by A'Hearn et al. (1995) or than the 2.74 (specific for G–Z) listed in their Table III. All these values are not associated with an unusually low abundance of C_2, C_3, NH, and NH_2, that is, regarding the gas-to-dust ratio, G–Z is a typical comet.

Acknowledgements. V. M. acknowledges the support of a MUTIS Fellowship from the Agencia Española de Cooperación Internacional (AECI). This research has been partially supported by the Spanish Ministerio de Ciencia y Tecnología under contract PNE-002/2000-C. We are very grateful to J. Crovisier for his constructive comments which have greatly improved the paper.

References

A'Hearn, M. F., Schleicher, D. G., Feldmann, P. D., Millis, R. L., & Thompson, D. T. 1984, AJ, 89, 579
A'Hearn, M. F., Birch, P. V., Feldmann, P. D., & Millis, R. L. 1985, Icarus, 64, 1
A'Hearn, M. F., Millis, R. L., Schleicher, D. G., Osip, D. J., & Birch, P. V. 1995, Icarus, 118, 223
Beaver, J. E., Wagner, R. M., Schleicher, D. G., & Lutz, B. L. 1990, ApJ, 360, 696
Biver, N., Crovisier, J., Davies, J. K., et al. 1999a, in abstract book for Asteroids, Comets and Meteors, 26–30 July 1999a, Cornell University, Ithaca
Biver, N., Bockelée–Morvan, D., Crovisier, J., et al. 1999b, AJ, 118, 1850
Biver, N., Bockelée–Morvan, D., Crovisier, J., et al. 2000, AJ, 120, 1554
Biver, N. D., Bockelée–Morvan, J. Crovisier, P., et al. 2002, Earth, Moon & Planets, Proc. IAU Coll., 186, in press
Bobrovnikoff, N. T. 1927, ApJ, 66, 439
Bockelée Morvan, D. 1997, in Molecules in Astrophysics: Probes and Processes, ed. E. F. Van Dishoek (Kluwer Academic, Dordrecht), pp. 219-235
Bockelée–Morvan, D., & Crovisier, J. 1985, A&A, 151, 90
Churyumov, K. I., & Rosenbush, V. K. 1991, Astron. Nachr., 312, 385
Cochran, A. L., & Barker, E. S. 1987, AJ, 93, 239
Combi, M. R., & Delsemme, A. H. 1980a, ApJ, 237, 633
Combi, M. R., & Delsemme, A. H. 1980b, ApJ, 237, 641
Dello Russo, N., Mumma, M. J., DiSanti, J. A., et al. 2000, Icarus, 143, 324
Ellis, T. A., & Neff, J. S. 2000, Icarus, 145, 591
Farnham, T., Schleicher, D., & A'Hearn, M. F. 2000, Icarus, 147, 180
Festou, M. C. 1981, A&A, 95, 69
Festou, M. C., Barale, O., Davidge, T., et al. 1998, BAAS, 30, 1089
Hanner, M. S., Veeder, G. J., & Tokunaga, A. T. 1992, AJ, 104, 386
Haser, L. 1957, Bull. Cl. Sci. Acad. R. Belg., 43, 740
Herbig, G. H. 1976, in The Study of Comets, ed. B. Donn, M. Mumma, W. Jackson, & M. F. A'Hearn, NASA SP-393, 136
Huebner, W. F., & Link, R. 1999, http://espsun.space.swri.edu/spacephysics/atomic/html/photoabs.htm
Huebner, W. F., Keady, J. J., & Lyon, S. P. 1992, Astrophys. Space Sci., 195, 1
Jewitt, D. C., & Meech, K. J. 1987, ApJ, 317, 992
Kiselev, N. N., Jockers, K., Rosenbush, V. K., et al. 2000a, Planet. Space Sci., 48, 1005
Kiselev, N. N., Jockers, K., & Rosenbush, V. K. 2000b, EMP 82-83, 141
Komitov, B., & Bonev, T. 1999, BAAS, 31, 1127
Konno, I., & Wyckoff, S. 1989, Adv. Space Res., 9, 163
Krasnopolsky, V. A. 1991, A&A, 245, 310
Landaberry, S. J. C., Singh, P. D., & de Freitas Pacheco, J. A. 1991, A&A, 246, 597
Lebedinets, V. N. 1991, Sol. Sys. Res., 25, 49
McFadden, L. A., A'Hearn, M. F., Fledman, P. D., et al. 1987, Icarus, 69, 329
Mumma, M. J., DiSanti, M. A., Dello Russo, N., Magee-Sauter, K., & Rettig, T. W. 2000, ApJ, 531, L155
Randall, C. E., Schleicher, D. G., Ballou, R. G., & Osip, D. J. 1992, BAAS, 24, 1002
Schleicher, D. G. 1983, Ph. D. Dissertation, Univ. of Maryland
Schleicher, D. G., Millis, R. L., & Birch, P. V. 1987, A&A, 187, 531
Schulz, R., A'Hearn, M. F., Birch, P. V., et al. 1993, Icarus, 104, 206
Schulz, R., McFadden, L. A., Chamberlin, A. B., A'Hearn, M. F., & Schleicher, D. G. 1994, Icarus, 190, 145
Singh, P. D., Huebner, W. F., Costa, R. D. D., Landaberry, S. J. C., & de Freitas Pacheco, J. A. 1997, Planet. Space Sci., 45, 455
Weaver, H. A., Chin, G., Bockelée-Morvan, D., et al. 1999, Icarus, 142, 482